International Journal of Chemical and Physical Sciences, ISSN:2319-6602
IJCPS Vol. 3 Special Issue – NCETNN Dec-2014
www.ijcps.org

Influence of Cu, Ce-doping on Gas Sensing Properties of Nanocrystalline SnO_2 thick Films

K.N. BAGAL[1], L.K. BAGAL[1], I.S. MULLA[2], S.S. SURYAVANSHI[3]

[1] K. B. P. Mahavidyalaya, Pandharpur 413304, India
[2] Emeritus Scientist National Chemical Laboratory, Pune 411008, India.
[3] School of Physical Sciences, Solapur University, Solapur 413255, India.
Email address: latika64_bagal@rediffmail.com

Abstract

The nanocrystalline powders of undoped, copper, cerium and copper with cerium–doped tin oxide were synthesized by facile co-precipitation method. The thick films of undoped and Cu, Ce, Cu with Ce–doped SnO_2 were formulated using screen-printing technique and further used to investigate their gas sensing properties towards LPG, ethanol, ammonia and acetone vapor. The crystal structure and microstructure of the sintered powders were characterized with X–ray diffractometer (XRD), scanning electron microscopy (SEM) and transmission electron microscopy (TEM). All the doped and undoped SnO_2 compositions revealed single phase solid solution formation. The doping of copper and cerium in SnO_2 improved the gas response due to the reduction in grain size. In comparison to LPG, ethanol, and ammonia the response towards acetone vapor increases markedly on simultaneous doping of Cu and Ce. The simultaneous doping of copper and cerium in tin oxide showed high gas response, quick response time and fast recovery time to acetone vapor at a working temperature of 250ºC. Further, the selectivity of sensor towards acetone with respect to other reducing gases (LPG, ethanol, ammonia) was studied. The results of gas sensing measurements reveal that the thick films deposited on alumina substrates using screen printing technique give selectively a high response of (87%) with quick response (20 sec) and fast recovery (~1 min) towards 100 ppm acetone at 250 ºC.

Keywords: SnO_2, Thick films, Screen-printing, Acetone vapor, (Cu+Ce) doping,

Introduction:

Metal oxide semiconductors are versatile materials due to their diverse properties and functionalities. Nanostructured materials have been of interest for gas sensing applications due to increased surface area and defect structure which have higher reactivity leading to better sensor characteristics. Among the known metal oxides used as sensors, tin oxide is the prominent and widely used metal oxide gas sensors due to its capability to detect various toxic, hazardous and flammable gases with high response, selectivity and good stability. SnO_2 being non-stoichiometric in nature is most suitable functional material for the gas sensing applications and the sensors based on it are extensively studied [1-6].

The sensors based on SnO_2 are widely used for the detection of oxidizing and reducing gases, also they have been used for the detection of volatile organic compounds (VOCs) [7, 8]. Reliability of SnO_2 is hampered by the poor selectivity and thus number of efforts has been made to improve its sensing characteristics. Several metals like Al, Zn, Cu, Fe, Ce, Co, Mn, etc. have been trialed out as additives in tin oxide [9-12].

Gas sensors have numerous applications in industries, environment monitoring and protection. Acetone is generally used as a chemical reagent in industry and it easily evaporates at room temperature. Human being may develop headache, fatigue if the concentration of acetone in air is higher than 10,000 ppm. The medical reports specify that the diabetic patients possess high acetone in their blood and saliva [13, 14] and hence they exhale high acetone. Therefore detection and measurement of acetone concentration is quite essential for our safety and health.

Experimental Procedure

Synthesis of undoped and doped SnO_2 nanoparticles and their characterization:

The undoped and doped SnO_2 powders were prepared by using the co-precipitation route. The precursors used for the synthesis were stannic chloride, copper sulphate and cerium nitrate. In synthesis of undoped SnO_2, appropriate quantity of stannic chloride ($SnCl_4 \cdot 5H_2O$) was dissolved in distilled water and the resulting precursor solution was stirred for half an hour on magnetic stirrer. The dilute ammonia solution (NH_4OH) was added drop-wise in the solution under stirring until the solution pH value remains 8. The resulting precipitate was then filtered and washed with distilled water for several times to remove chloride ions [15]. The resulting product was followed by calcinations in air at 450ºC for 2 h. This sample was labeled as S1. Thick films were prepared by screen-printing technique as described by Nitta and Haradome [16]. The paste was screen-printed on an alumina substrate (10 x 20 mm) by using screen-printing technique. Samples S2, S3 and S4 were prepared as per Table 1.

Table 1: Sample identification for SnO_2

Sample code	Composition
S1	Undoped SnO_2using co-precipitation method
S2	98wt% $SnCl_4$ + 2 wt% $CuSO_4$
S3	96wt% $SnCl_4$ + 4wt% $Ce(NO_3)_3$
S4	94wt% $SnCl_4$ + 2wt% $CuSO_4$ + 4wt% $Ce(NO_3)_3$

The X-ray diffraction (XRD) pattern of the samples were obtained on BRUKER AXS D8-Advanced X-ray diffractometer using Cu-Kα (λ=1.5418Å) radiation at 2θ values between 20º and 80º. The surface morphology of all the compositions were obtained using Model JSM-6360 scanning electron microscope instrument. The percentage of constituent elements was evaluated by the energy dispersive X-rays (EDS) technique. The transmission electron microscopic (TEM) analysis and selected area electron diffraction (SAED) were performed on the Philips CM 200 FEG microscope equipped with a field emission gun at an accelerating voltage of 200 kV, with a resolution of 0.24 nm. The UV-absorption spectra were performed using JASCO (Model V-670) UV-VIS-NIR spectrophotometer. The spectra were taken in the wavelength range of 200-1000 nm for studying the optical band-gap of the samples.

Gas response measurement:

The sintered screen-printed thick film sensors were tested for gas sensing properties. Digital Nanometer Model DNM-121 and ScienTECH variable power supply ST4074 were used to measure the change in resistance of the sample. Conducting silver paste was used to make ohmic contacts on both ends of thick film and measurements were taken using the gas sensing set-up described earlier [17]. The gas sensing characteristics of all the samples were investigated towards four different gases (LPG, acetone, ethanol and ammonia) under identical experimental conditions. The resistance of the sample in presence of air and in presence of test gas was measured. The experiment was repeated twice to check the repeatability of the sensor. The gas response was defined as $S = (R_a - R_g)/R_a$, where, R_a is resistance of sensor in air and R_g is resistance in presence of test gas.

Results and Discussion

Characterization of the sensors:

The XRD patterns of sintered samples S1, S2, S3, and S4 are shown in Fig.1. All the diffraction peaks have been indexed to the tetragonal rutile structure of SnO_2 with lattice constants which are in good agreement with the reported values (a = 4.750Å and c = 3.196Å) from JCPDS card (No. 77-0451). For Cu, Ce-doped SnO_2, no diffraction peaks of copper oxide or cerium oxides were observed, suggesting that Cu^{2+}, Ce^{3+} ions get uniformly substituted into the Sn^{4+} sites. Moreover, the major diffraction peaks in case of doped samples (S2, S3, and S4) shift slightly towards smaller diffraction angle as compared to S1. The increase in lattice parameters in case of S2, S3, and S4 is attributed to the large ionic radii of Cu^{2+} (73 pm), Ce^{3+} (115 pm) which substitutes the smaller ionic radius of Sn^{4+} (71 pm) ion.

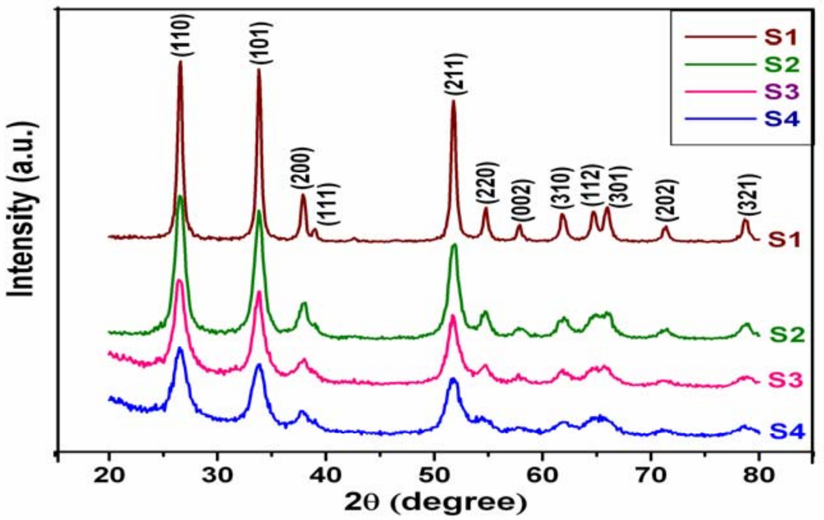

Fig. 1. XRD pattern of undoped (S1), Cu–doped (S2), Ce–doped (S3) and (Cu+Ce)–doped SnO_2 (S4).

The crystallite size D, for a sintered composition was calculated from the Scherrer formula:

$$D = \frac{0.9\lambda}{\beta \, \mathrm{Cos}\theta} \qquad (1)$$

where λ, β and θ are the X-ray wavelength, the full width at half maximum (FWHM) of the diffraction peak, and the Braggs diffraction angle, respectively. The reduction in peak intensity and increase in width broadening for S2, S3, and S4 support lowering in crystallite size and thus confirms the role of Cu and Ce as grain growth inhibitors [18].

Fig. 2 depicts the SEM images of sintered thick films of all the samples. The microstructure reveals formation of the agglomerated grains with remarkable porosity which facilitates gas response. The Cu with Ce–doped SnO_2 sample S4 possesses maximum porosity as compared to the other samples and it provides maximum surface area for adsorption of oxygen and test gases. Such high surface area available for the adsorption of test gas plays an important role in gas response. The elemental composition obtained from the EDS spectrum confirms the presence of Cu, Ce, Sn and oxygen.

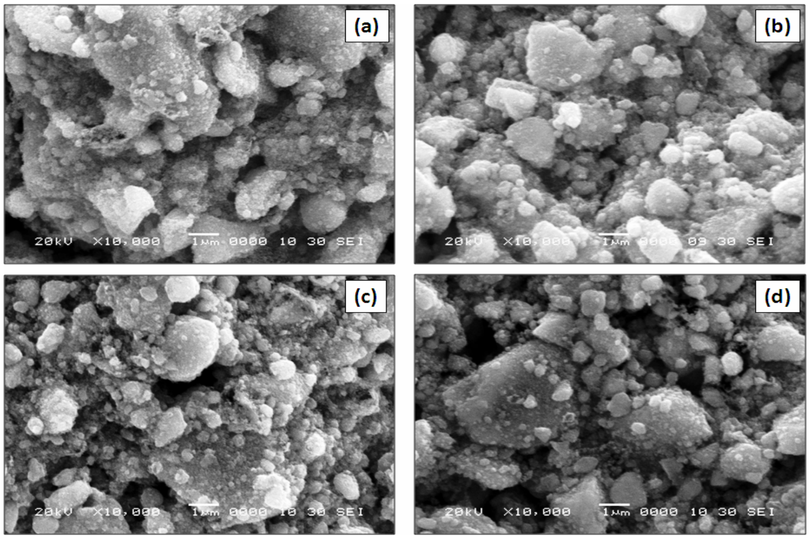

Fig. 2. SEM image of the surface of SnO_2 thick films: (a) undoped SnO_2 (b) Cu–doped SnO_2 (c) Ce–doped SnO_2 (d) (Cu+Ce)–doped SnO_2.

It is well known that gas-sensing properties of a metal oxide strongly depend on its morphological features. A high surface area facilitates the chemisorptions process by increasing the adsorption and desorption rates. It has been shown that smaller grain size increases gas response. More information regarding the structure and morphology were obtained from the TEM microstructure of the samples..

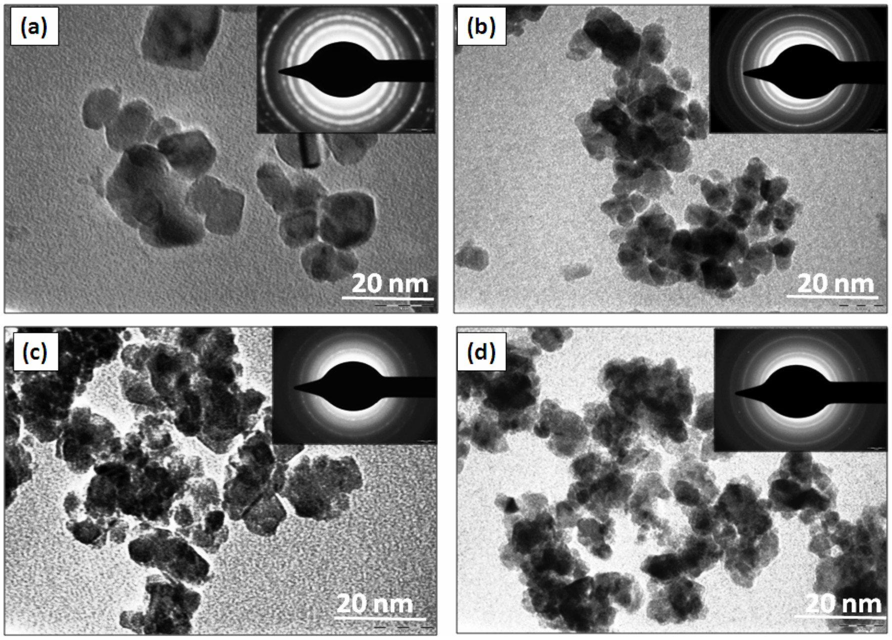

Fig.3. TEM image with SAED pattern of SnO_2 thick films: (a) undoped SnO_2 (b) Cu– doped SnO_2 (c) Ce–doped SnO_2 (d) (Cu+Ce)–doped SnO_2.

The TEM micrographs, Fig. 3((a)-(d)) shows particle size and type of morphology. The TEM image reveals that doped tin oxide particles are smaller than undoped samples. The Cu, Ce, and both-doped SnO_2 show agglomerated grains, having a wide particle size distribution. The average particle size was about 5-9 nm. The Selected Area Electron Diffraction (SAED) pattern (shown in inset) of an isolated particle shows bright rings corresponding to the lattice planes of SnO_2 structure which are in good agreement with the X-ray diffraction pattern. The average particle size matches well with that calculated by the Scherrer equation from the XRD peaks.

The UV- absorption spectra of undoped and doped SnO_2 are shown in Fig.4 and the band gap energy values were calculated from the absorption edge corresponding to each sample. The optical band gap Eg was calculated from the plot of $(\alpha h\nu)^2$ versus $(h\nu)$ as shown in Fig.4. By extrapolating the linear part of the plot to $\alpha=0$, the optical band gap of 4.1 eV was estimated for undoped SnO_2, while the optical band gap decreases with respective doping of Cu (3.79 eV), Ce (3.66 eV), and simultaneous Cu with Ce (3.60 eV) in SnO_2.

The doping of Cu, Ce, and Cu with Ce in SnO_2 resulted into the decrease in band gap which reflected as red shift in absorption spectra to a certain minimum value. The observed shift in band-gap values with dopants may be attributed to the change in energy eigen values as a result of perturbation potential due to exchange interaction.

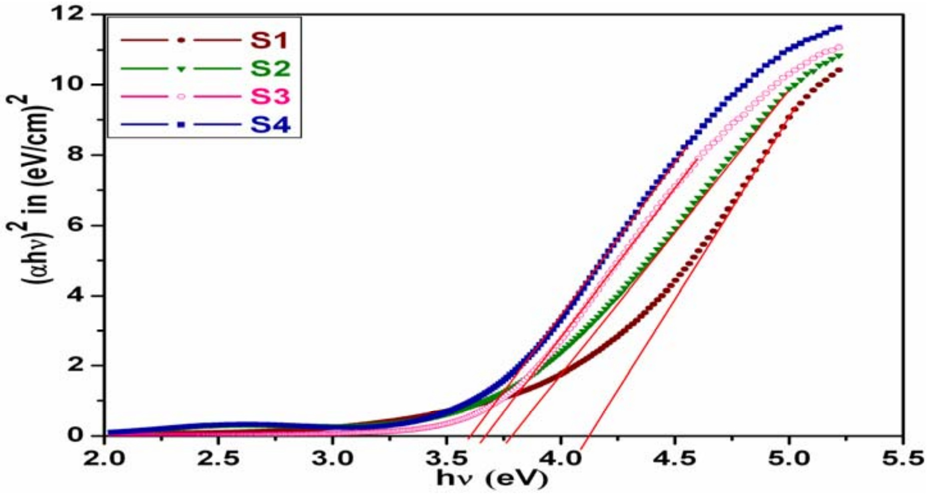

Fig. 4. UV spectra of undoped , Cu, Ce and (Cu+Ce)–doped SnO_2.

Gas sensing properties:

We have examined the response of S1, S2, S3, and S4 towards acetone at 500 ppm concentration at various operating temperatures and are shown in Fig.5. From figure it is evident that the response and operating temperature are influenced by doping of Cu, Ce. Each sensor exhibits highest response to acetone vapor at its optimal temperature. The S4 shows maximum response of 87% at 250ºC, which is highest among all the other samples S1 (39%), S2 (59%), S3 (65%). Smaller grain size of S4 brings a larger specific surface area and a higher surface activity for adsorption of oxygen and reaction with test gas, which induces a larger change in the electrical conductivity of the sensor and eventually a higher sensor response. The decrease in the optimal operating temperature in the present investigation can be due to the synergistic effects induced as a result of co-doping of Cu and Ce in SnO_2.

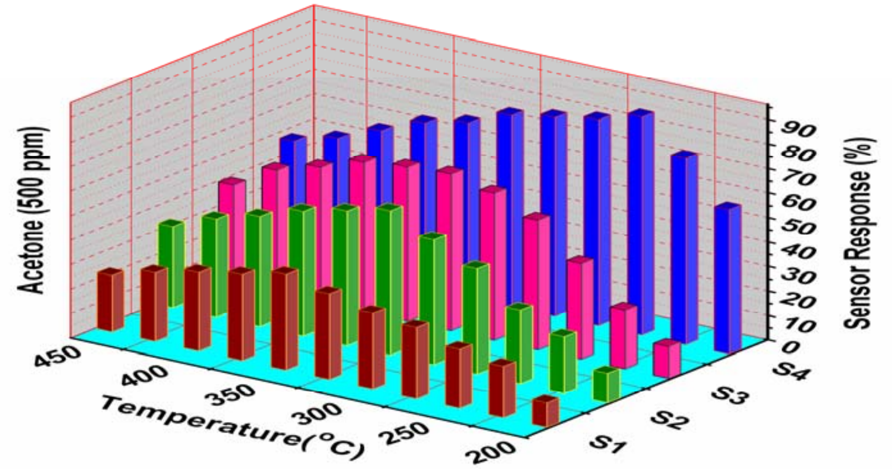

Fig. 5.Variation in sensor response towards fixed concentration (500 ppm) of acetone vapor measured at different temperature.

The response of sintered thick films of S1, S2, S3 and S4 towards various test gases at 100 ppm was studied at an optimum temperature of 250 ºC. It can be seen from Fig. 6 that all the samples show high response and selectivity towards acetone in comparison with the other gases like LPG, ethanol and ammonia. It is found that for sample S4 the response is about 87% which is four times larger than that of S1 (18%). Thus S4 sample has proved to be the potential candidate for acetone detection at low concentration and relatively moderate operating temperature.

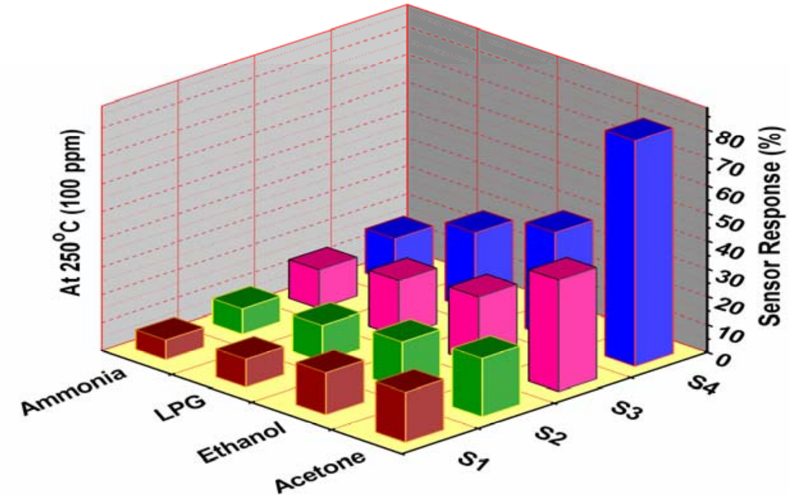

Fig. 6. Response (%S) of undoped and doped SnO_2 samples at 250ºC for 100 ppm concentration of various gases.

The change in gas response as a function of acetone concentration for all the samples of SnO_2 at their optimum operating temperature is shown in Fig.7. It illustrates that the gas response increases with increase in concentration of acetone. Beyond 500 ppm the response of the S4 is found to be saturated, however the saturation limit in case of other samples (S1, S2 and S3) is at 1000 ppm. At lower gas concentrations the unimolecular layer of gas molecules forms on the surface of the sensor, which interacts more actively and thus might be giving larger response. The multilayer of gas molecules formed on the sensor surface at higher gas concentrations would result in saturation of response beyond 1000 ppm.

The transient response characteristics of all the samples exposed to 100 ppm acetone concentration at an operating temperature of 250 ºC are shown in Fig.8. From figure it is obvious that, as we go from S1 to S4 the sensor response is found to enhance significantly, which is attributed to the change in morphology and reduction in crystallite size of the sample with doping, which facilitates the adsorption of oxygen significantly. In case of S4, the number of active adsorption sites for oxygen is high as compared to S1, S2 and S3. The adsorption of oxygen on the surface increases the resistance of the sensor material due to transport of electrons from conduction band to adsorbed oxygen which results in increase in gas response.

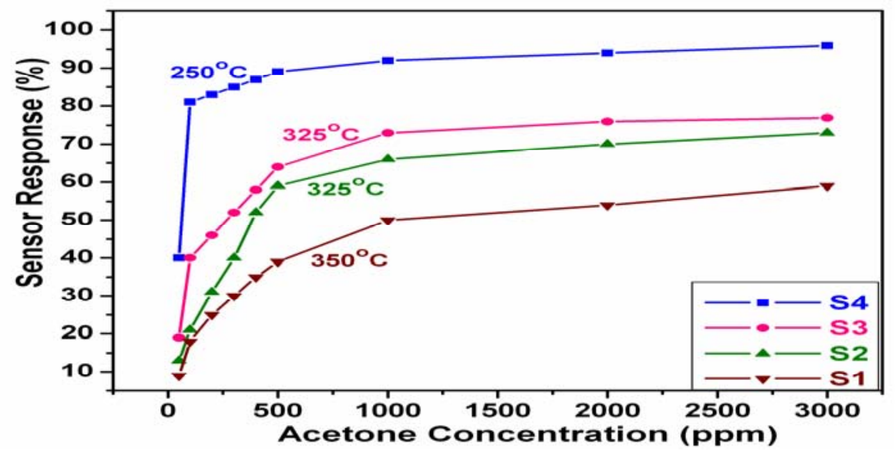

Fig. 7. Variation in sensor response to different concentrations of acetone vapor measured at the optimum operating temperatures.

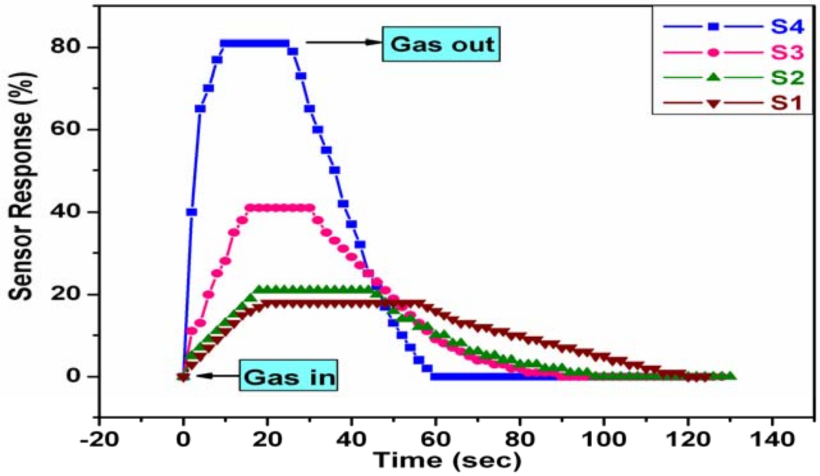

Fig. 8. Transient response characteristics of undoped and doped SnO_2 exposed to 100 ppm acetone vapor at optimal operating temperatures.

Conclusions

Undoped, copper, cerium, and copper with cerium doped nanocrystalline tin oxide powders were successfully synthesized by co-precipitation route. The incorporation of Cu, Ce and Cu with Ce is found to introduce significant structural and morphological changes in SnO_2. The substitution of Sn ions by Cu or Ce ions modifies the surface of base material by providing larger surface area and reactivity for adsorption of oxygen. The reduction in grain size is due to incorporation of these metal oxides which favors the interaction between the material surface and the test gas. The sensor S4 (Cu with Ce-doped SnO_2) exhibited selective acetone response with rapid response (20 sec) and fast recovery (~1 min) at 100 ppm. The simultaneous doping of Cu and Ce in SnO_2 showed profound effect on the gas sensing properties hence it can be used as promising candidate for the fabrication of high-performance acetone gas sensor.

References:

1. D. Kohl, *Sens. Actuators. B* 18 (1989) 71.
2. N. Brasan, J.R. Stetter, M. Findlay, W. Gopel, *Sens. Actuators* B 66 (2000) 31.
3. J. Tamaki, T. Maekqwa, N. Miura, N. Yamazoe, Sens. Actuators B 26–27, 49 (1995).
4. G. Zhang, M. Liu, *Sens. Actuators*. B 69, 144 (2000).
5. S.T. Jun, G.M. Choi, *Sens. Actuators.* B 17, 175(1994).
6. D.H. Yoon, J.H. Yu, G.M. Choi, *Sens. Actuators. B* 46, 15 (1998).
7. N.G. Patel, P.D. Patel, V.S. Vaishnav, *Sens. Actuators B* 96, 180 (2003).
8. F. Hellegouarc'h, F. Arefi-Khonsari, R. Planade, J. Amouroux, *Sens. Actuators B* 73, 27(2001).
9. G. Zhang, M. Liu, *Sens. Actuators B* 69, 144(2000).
10. P. Ivanov, E. Llobet, X. Vilanova, J. Brezmes, J. Hubalek, X. Correig, *Sens. Actuators B* 99, 201 (2004).
11. N. Yamazoe, Y. Kurokawa, T. Seiyama, *Sens. Actuators B* 4, 283(1983).
12. F. Pourfayaz, Y. Mortazavi, A. Khodadadi, S. Ajami, *Sens. Actuators B* 130 (2008)
13. S.S. Likhodii, K. Musa, S.C. Cunnane, *Clin. Chem*. 48, 115 (2002).
14. N. Makisimovich, V. Vorotyntsev, N. Nikitina, O. Kaskevich, P. Karabun, F. Martynenko, *Sens. Actuators B* 36, 419 (1996).
15. A. Mosquera, J.E. Rodringuez-Paez, J.A. Varela, P.R. Bueno, *J. Eur. Ceram. Soc.* 27, 3893-3896(2007).
16. M. Nitta, M. Haradome, *IEEE Transactions, Electron Devices ED*-26, 247-249 (1979).
17. R.C. Pawar, J.S. Shaikh, A.V. Moholkar, S.M. Pawar, J.H. Kim, J.Y. Patil , S.S. Suryavanshi, P.S. Patil, *Sensors and Actuators B* 151, 212-218 (2010).
18. A. Srivastava, Rashmi, and K. Jain, *Mater. Chem. Phys.*105, No.**2-3**, 385-390 (2007).